Computerized Medical Imaging and Graphics xxx (xxxx) xxx–xxx

Contents lists available at ScienceDirect

Computerized Medical Imaging and Graphics

journal homepage: www.elsevier.com/locate/compmedimag

Intensity-based volumetric registration of magnetic resonance images and whole-mount sections of the prostate

Are Losnegård[a,b], Lars Reisæter[a], Ole J. Halvorsen[c,g], Christian Beisland[b,d], Aurea Castilho[f], Ludvig P. Muren[e], Jarle Rørvik[b,a], Arvid Lundervold[f,a,*]

[a] Department of Radiology, Haukeland University Hospital, Bergen, Norway
[b] Department of Clinical Medicine, University of Bergen, Norway
[c] Centre for Cancer Biomarkers CCBIO, Department of Clinical Medicine, University of Bergen, Norway
[d] Department of Urology, Haukeland University Hospital, Bergen, Norway
[e] Department of Medical Physics, Aarhus University Hospital, Denmark
[f] Department of Biomedicine, University of Bergen, Jonas Lies vei 91, 5009 Bergen, Norway
[g] Department of Pathology, Haukeland University Hospital, Bergen, Norway

ARTICLE INFO

Keywords:
Image registration
MR imaging
Prostate cancer
Whole-mount sections

ABSTRACT

Objective: Magnetic Resonance Imaging (MRI) of the prostate provides useful *in vivo* diagnostic tissue information such as tumor location and aggressiveness, but *ex vivo* histopathology remains the ground truth. There are several challenges related to the registration of MRI to histopathology. We present a method for registration of standard clinical T2-weighted MRI (T2W-MRI) and transverse histopathology whole-mount (WM) sections of the prostate.

Methods: An isotropic volume stack was created from the WM sections using 2D rigid and deformable registration combined with linear interpolation. The prostate was segmented manually from the T2W-MRI volume and registered to the WM section volume using a combination of affine and deformable registration. The method was evaluated on a set of 12 patients who had undergone radical prostatectomy. Registration accuracy was assessed using volume overlap (Dice Coefficient, DC) and landmark distances.

Results: The DC was 0.94 for the whole prostate, 0.63 for the peripheral zone and 0.77 for the remaining gland. The landmark distances were on average 5.4 mm.

Conclusion: The volume overlap for the whole prostate and remaining gland, as well as the landmark distances indicate good registration accuracy for the proposed method, and shows that it can be highly useful for registering clinical available MRI and WM sections of the prostate.

1. Introduction

Magnetic Resonance Imaging (MRI) is used increasingly for detection, characterization and staging of prostate cancer (PCa) (Barentsz et al., 2012; Kitajima et al., 2010; Rosenkrantz et al., 2016; Steenbergen et al., 2015). Histopathology is regarded as the ground truth for diagnosis and assessing tumor aggressiveness. Therefore, accurate registration of MRI and histopathology whole-mount (WM) sections is important to allow comparisons between the two modalities (Le Nobin et al., 2014; Reisæter et al., 2015; Singanamalli et al., 2015; Tiwari et al., 2013). Computer aided diagnosis (CAD) systems (Borren et al., 2014; Ginsburg et al., 2015; Litjens et al., 2015) applying multiparametric MRI (mpMRI) and histopathology are dependent on accurate co-registration, both for development and evaluation.

Registration of MRI and histopathology in the prostate is challenging because of the differences between the two modalities (Commandeur et al., 2015; Stille et al., 2013; Xiao et al., 2011). The T2-weighted (T2W) MRI sequence has good in-plane resolution, but still much lower resolution than digitally scanned WM sections. If we compare the slice-thicknesses and between-slice-distances, voxels in clinical MRI scans are generally thick and separated by a small gap, while WM sections are very thin and separated with a larger intersection distance. When preparing the WM sections after radical prostatectomy, the prostate is often deformed compared to the *in vivo* MR imaged prostate, and tissue may be damaged. It is also a great challenge to cut the WM sections in the exact same plane as the MRI transverse plane. Transversal WM sections are often only available for the middle part of the prostate, as the base and apex are usually cut sagitally.

* Corresponding author at: Department of Biomedicine, University of Bergen, Jonas Lies vei 91, 5009 Bergen, Norway.
E-mail address: arvid.lundervold@biomed.uib.no (A. Lundervold).

https://doi.org/10.1016/j.compmedimag.2017.12.002
Received 10 February 2017; Received in revised form 9 December 2017; Accepted 12 December 2017

In previous methods for registration of whole-mount sections and *in vivo* MRI of the prostate, varying types of data and methods have been applied. A method for finding slice correspondence in the two modalities was developed by Xiao et al. (2011). Mazaheri et al. (2010) manually found corresponding slices and applied a 2D registration method. Commandeur et al. (2015) used distance maps derived from delineated structures to optimise the registration. Gross prostate specimen has been included in several studies (Groenendaal et al., 2010; Orczyk et al., 2013; Starobinets et al., 2014) to compensate for tissue damage during the preparation of the whole-mount sections. Additional *ex vivo* MRI has been added as an intermediate step to facilitate the registration (Kimm et al., 2012; Nir et al., 2014; Park et al., 2008). Fiducial markers have been used to guide the registration (Gibson et al., 2012; Ward et al., 2012), while others have used manually defined landmarks for the same purpose (Kalavagunta et al., 2015; Starobinets et al., 2014; Zhan et al., 2007). Methods for creating histology volumes from slices have been studied previously in Commandeur et al. (2015), Stille et al. (2013), Rusu et al. (2015).

In this work we present a new registration method. The aim was to enable 3D volume registration of clinically available *in vivo* T2W-MRI acquisitions and histopathology WM sections, where the latter modality may (i) be sparse, (ii) cover only the middle part of the prostate, and (iii) differ in cutting angle compared to the MRI imaging plane. The method was designed to overcome these challenges without prior knowledge of the slice correspondences or using control points. Our approach involves two main steps. First, we create a histopathology prostate volume from the WM sections using rigid registration, where a dense histology volume is obtained using interpolation combined with deformable registration. Next, we apply a sequence of algorithms for registration of the T2W-MRI prostate volume to the histopathology prostate volume.

2. Material and methods

2.1. Patient material

MRI acquisitions and histopathology WM sections from 12 patients (age range: 43–70 years) with histology-proven prostate cancer who underwent radical prostatectomy at our hospital were included in this work. Our institutional review board approved the study and all patients gave their written informed consent.

2.2. Histopathology

WM sections of the prostate were prepared from the radical prostatectomy specimens. The formalin-fixed prostate was cut in the transverse plane perpendicular to the rectal surface using a slicing device, guiding the knife at 5 mm intervals, and 5 µm sections from these paraffin blocks were mounted on glass slides and stained with hematoxylin and eosin. The slides were digitally scanned with a flatbed scanner (Epson Expression 750XL, 4800 dpi, 0.0053 × 0.0053 mm pixel size). The base and apex of the prostatectomy specimens, being cut into multiple small blocks in the sagittal and parasagittal planes, were not used in this study. Using ink, the malignant tumor foci, prostatic capsule (whole prostate gland; WG) and peripheral zone (PZ) (including the central zone) was delineated on the glass slides by an experienced uropathologist prior to digitization.

2.3. MR imaging

Turbo spin echo T2W-MRI recordings were acquired on a 1.5 T scanner (Avanto; Siemens Medical Systems, Erlangen, Germany) with an integrated endorectal and pelvic phased-array coil (MR Innerva; Medrad, Pittsburgh, PA, USA), covering the entire prostate gland. Repetition time, echo time, and flip angle was 4840 ms, 84 ms, and 150°, respectively. The voxel size was 0.63 × 0.63 × 3.6 mm^3 with 24 slices of thickness 3.0 mm and inter-slice gap of 0.6 mm. The T2W-MRIs were recorded together with other sequences (T1W, DWI, DCE-MRI) in a multi-parametric MRI examination (mpMRI). However, only the T2W-MRI recordings were used in this image registration study, because this is the sequence providing the most detailed anatomical information with good contrast and high signal-to-noise ratio. The T2W-MRI slice acquisitions are subsequently referred to as the MRI volumes.

2.4. Registration of MRI volumes to the whole-mount histological sections

The multimodal image registration was performed in three successive steps: (i) alignment and interpolation of the separate histological sections being scanned, (ii) manual delineation and re-sampling of the imaged prostate gland in the MRI volume, and (iii) intensity based co-registration of the cropped MRI volume to the histological sections obtained in (i). These steps are explained in the following.

2.4.1. Alignment of the separate whole-mount histological sections

To create a histopathology volume, the WM sections were stacked together using 2D registration. The WM sections are usually of different sizes, which may be caused by deformations during the preparation, but it may also reflect true differences in prostate diameter at different levels between the base and the apex. Using deformable registration at this step could cause all the resulting slices erroneously to have the same diameter, therefore only rigid registration was applied here. We employed the mean square difference as similarity metric, commonly used for single-modality image registration. The middle slice (σ_m) was used as the reference image. The neighbouring slices (σ_{m-1} and σ_{m+1}) were registered to σ_m, which were denoted σ^r_{m-1} and σ^r_{m+1}, respectively. Next, σ_{m-2} was then registered to σ^r_{m-1}, and σ_{m+2} was registered to σ^r_{m+1}, and denoted σ^r_{m-2} and σ^r_{m+2}, respectively. This process was continued for all subsequent neighbouring WM sections. The registered slices and the reference slice were stacked together in a volume, using the *a priori* slice thickness and distance (c.f. Algorithm 1 and Fig. 1).

Algorithm 1. WM volume stack from separate WM sections

1: Select the middle transverse WM section, denoted σ_m
2: Register the neighbouring WM sections, σ_{m+1} and σ_{m-1}, to σ_m, using 2D rigid registration, resulting in σ^r_{m+1} and σ^r_{m-1}.
3: Register σ_{m-2} to σ^r_{m-1} and σ_{m+2} to σ^r_{m+1}, and so forth.
4: Create a stack σ of the registered WM sections, $\sigma = \{\sigma^r_{m-n}, ..., \sigma^r_{m-1}, \sigma_m, \sigma^r_{m+1}, ..., \sigma^r_{m+n}\}$, using 5 mm slice distance and 5 μm slice thickness.

The resulting WM volume stack describing the prostate volume using the available WM sections, may still not be optimal for registration purpose, being sparse and consisting of anisotropic voxels. We used interpolation between the slices to obtain a dense 3D WM volume stack. To avoid edge artefacts which may occur when interpolating between WM sections with different sizes, and to obtain smooth transitions, we combined 2D deformable registration with linear interpolation. For all adjacent slices, e.g. σ_m and σ_{m+1}, we found the 2D deformation field (Df_m). A set of $n = 1, \ldots, j-1$ interpolated slices ($\sigma_{m+\frac{n}{j}}$) were then created using the deformation field *Df* and linear interpolation weights. The functions *imregdemons* and *imwarp* (Matlab R2016b) were used for this purpose. Finally, the originally high in-plane resolution was reduced towards the MRI in-plane resolution, i.e. half the in-plane voxel side length. The number of interpolated slices, *n*, were set such that the slice distance matched this resolution. In this way, the final WM volume stacks had isotropic cubic voxels with side length 0.31 mm.

2.4.2. Preprocessing MRI

To simplify the multimodal registration task, the MRI volumes were processed before the registration in the following manner. First, manual delineation of the prostate was performed to crop the volume of interest, using the ITK-SNAP software (itksnap.org) (Yushkevich et al.,

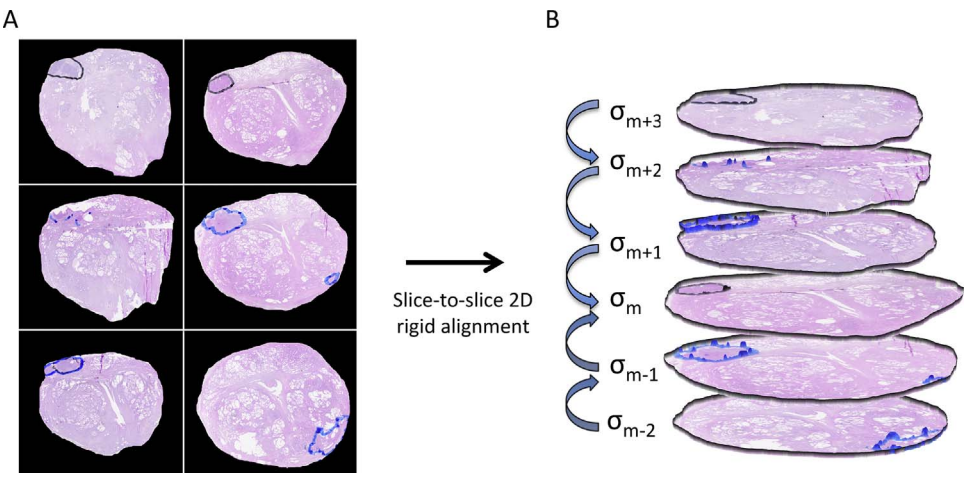

Fig. 1. Obtaining a histological volume stack (B, sagittal view) from separate whole-mount sections, scanned with a flatbed scanner (A, transverse view).

Table 1
Dice Coefficients for WG, PZ and RG and landmark distances (given in mm) for the 12 patients. Overall means and standard deviations in the last row.

Patient	WG	PZ	RG	Landmark distances (mm)
1	0.91	0.51	0.84	11.6 ± 2.9
2	0.97	0.72	0.86	4.3 ± 0.7
3	0.96	0.79	0.79	6.2 ± 1.1
4	0.89	0.80	0.56	4.0 ± 1.9
5	0.94	0.80	0.72	3.3 ± 0.7
6	0.94	0.60	0.60	5.5 ± 2.2
7	0.94	0.63	0.85	7.4 ± 1.9
8	0.97	0.55	0.72	2.7 ± 0.4
9	0.96	0.63	0.73	3.3 ± 1.7
10	0.97	0.57	0.86	5.3 ± 1.7
11	0.91	0.39	0.83	5.9 ± 0.1
12	0.97	0.54	0.93	5.4 ± 5.1
$\mu \pm \sigma$	0.94 ± 0.03	0.63 ± 0.13	0.77 ± 0.11	5.4 ± 2.4

2006). Then, the cropped volume was resampled to isotropic voxels with a voxel side length of 0.31 mm, being half of the original in-plane voxel size, and equal to the voxel size of the WM volume stack.

2.4.3. Registration of MRI to WM volume stack

The MRI and WM volume stacks were stored in the nifti file-format, with the advantage of single 3D volume files and keeping the correct header information such as orientation. We used the Advanced Normalization Tools (ANTS, http://www.picsl.upenn.edu/ANTS/) (Avants et al., 2011) to align each patient's prostate MRI and WM volume stack. After an initial alignment of the geometric centres, registration was run as a combination of affine registration (gradient step size = 0.1) followed by deformable registration using the B-spline symmetric normalization methodology (*BSplineSyN*). The parameters for *BSplineSyN* was set to 0.1,3,0 (gradientStep, updateFieldMeshSizeAtBaseLevel and totalFieldMeshSizeAtBaseLevel), and $4 \times 2 \times 1$ shrinkage level was used. Mutual information (MI) (Collignon et al., 1995; Viola and Wells, 1995), which is generally regarded as optimal for multi-modal image registration, was used as similarity metric. Computational time was 2–3 min on a 2.7 GHz, quad core, 16 GB, MacBook Pro.

2.5. Evaluation of the registration method

To assess the registration accuracy, we used volume overlap and distances between landmarks. Volume overlaps were measured using manual segmentations in WM sections, performed by an experienced uropathologist (O.J.H), and in MRI by an experienced radiologist (L.R). The segmented structures were the whole prostate gland (WG) and the peripheral zone (PZ), and we additionally used the remaining gland (RG), which encompassed the whole prostate gland excluding the peripheral zone and central zone. The affine transformations and deformation fields obtained during registration were applied to these segmented volumes, and then compared using the Dice Coefficient (DC) (Dice, 1945):

$$\mathrm{DC} = \frac{2|X \cap Y|}{|X| + |Y|}. \quad (1)$$

Distances between corresponding landmarks in the transformed MRI volumes and the reference WM volume stack were computed using the Hausdorff distance and also used to quantify the registration accuracy. As landmarks we used hyperplastic noduli, tumor foci and the seminal colliculus that were possible to identify both in the MRI volumes and the WM sections. The landmarks were defined in 3D, with the ability of measuring the registration accuracy not only in-slice, but also along the z-axis.

3. Results

The volume overlaps (DCs) for the whole prostate (WG), peripheral zone (PZ) and remaining gland (RG) as well as the landmark distances overall and for each patient are shown in Table 1. We found that our registration approach resulted in a very high DC for the WG, i.e. 0.94 on average. We obtained a high mean DC of 0.77 for the RG. For the PZ, the results were not as good, with an average DC of 0.63. Fig. 2 illustrates the manual segmentations of the PZ and WG in one of the patients in both MRI and pathology, as well as the resulting overlaps after registration.

The mean distance between the landmarks after registration was 5.4 mm, which we regarded as good, considering the 5 mm slice distance between the WM sections and that the landmarks were defined in 3D. Among the 12 patients only one patient had relatively large registration error (patient no. 1). A landmark in one of the patients (patient no. 4) is shown in Fig. 3 together with the resulting position after registration. As can be seen in Fig. 3 C, transversal view shows high accuracy. However, Fig. 3 D and E reveal a registration error along the z-axis. The error was 5 mm for this landmark, which equals the distance between the WM sections.

Fig. 4 allows for visual slice-wise inspection of the registration results for one patient (patient no. 8). As can be seen in Fig. 4, the outer prostate surface was aligned very well in most slices. In the most inferior and superior slices (first and last row) the surfaces were partly mis-aligned, which was likely due to ruptured WM sections (first row) and large deformations (last row). The urethra was very well aligned, as can be seen in the checkerboard images in rows 2–4.

Illustrations of the registration result in sagittal and coronal views

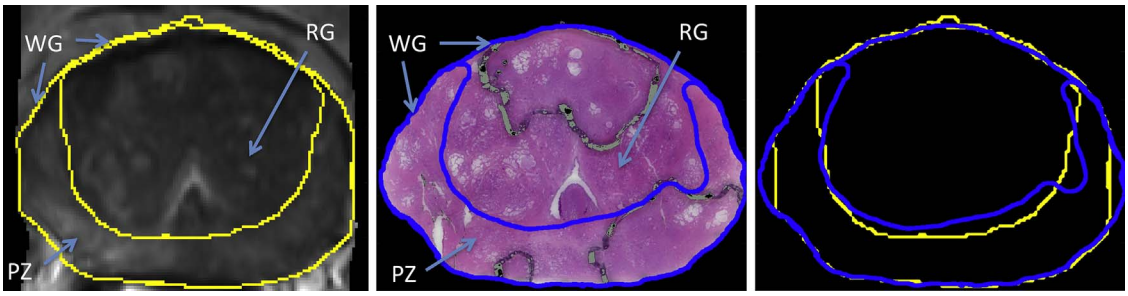

Fig. 2. Manual segmentations of the WG and PZ as well as the RG for patient no. 8. in one of the MRI slices (left), in the corresponding WM section (middle), including overlap of the masks after registration (right).

are given in Fig. 5. Since the WM sections covered the middle part of the prostate only, Fig. 5 demonstrates that our registration approach was able to reconstruct this feature correctly. Also, Fig. 5 shows the registration result for this patient with regards to slice angle deviations, visible both in the coronal and sagittal views.

4. Discussion

The development of mpMRI has brought improved *in vivo* detection, characterization and staging of prostate cancer (Tiwari et al., 2013; Turkbey et al., 2009). The mpMRI-based radiology scoring system PI-RADS (Barentsz et al., 2012) is applied clinically and is under development for improved performance. Systems for computer-aided detection (CAD) based on mpMRI are being developed and tested (Litjens et al., 2015; Vos et al., 2012), as well as studies on mpMRI-derived cancer biomarkers (Borren et al., 2014; Singanamalli et al., 2015). For all these applications, histopathology remains the ground truth. To enable accurate and systematic comparison of mpMRI and histopathology, methods for registration between MRI and histopathology WM sections are of great interest. In this work, we have developed and tested a registration method for clinically available *in vivo* MRI recordings and WM sections of the prostate. Our registration method was applied to axial T2W-MRI and transverse histopathology WM sections of the prostate, with good accuracy and promising results, obtained in 12 patients from clinical routine. The WM sections were stacked together to a volume using 2D rigid registration and interpolation. The segmented MRI prostate volume was resampled and registered to the WM volume stack using a combination of affine and deformable registration to find the imaging plane and set of slices corresponding to the set of WM sections and to correct for possible deformations.

The main advantages of our registration method is that (i) it can be applied to clinically available T2W-MRI and sparse WM sections, (ii) it is relatively easy to implement and computational time is 2–3 minutes on a MacBook Pro (2013 version), and (iii) it does not require manual slice correspondence or control points to guide the registration, which can be a difficult and time-consuming task. The method was also designed to tolerate differences between the MRI imaging plane and the cutting plane used to make the WM sections.

We evaluated the performance of our method using volume overlap and distances between landmarks. Manual segmentations of the prostate, the peripheral zone and the remaining gland were used to measure the volume overlap. Since volume overlap is not always an accurate measure alone, especially for spherically shaped objects, we combined it with distances between landmarks. These were hyperplastic noduli, tumor foci and the verumontanum that were identified in both the MRI and WM sections. The distances between these landmarks after registration give a good indication of registration accuracy in 3D.

More specifically, our registration method achieved high volume

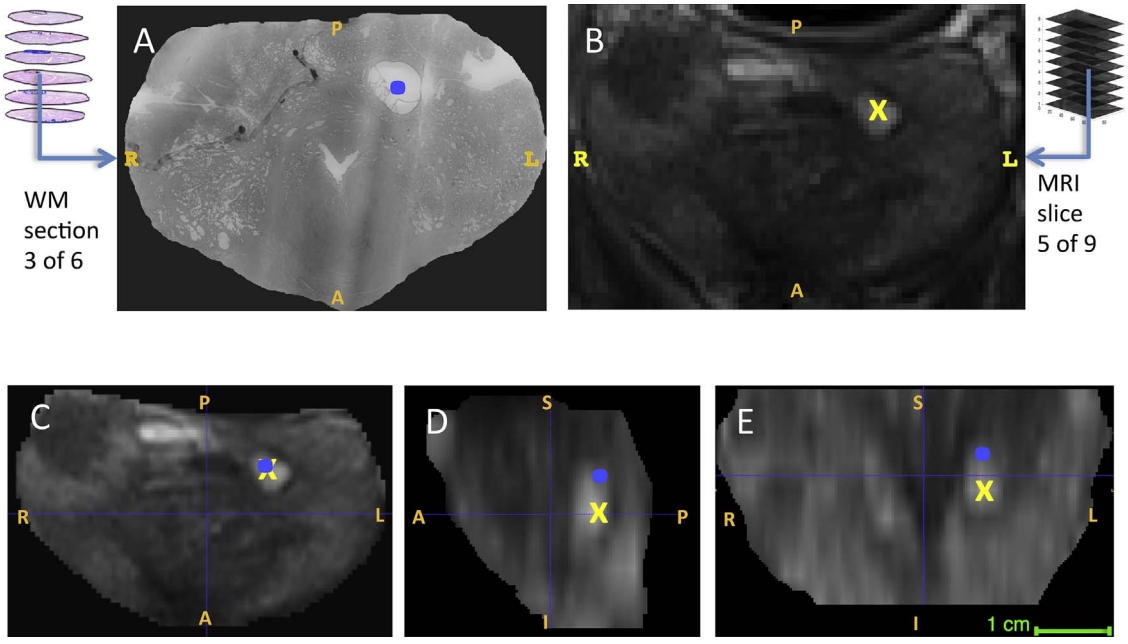

Fig. 3. Example of landmark used to assess the registration accuracy. For this patient, WM section 3 of 6 (A) was used to define a landmark in pathology (blue dot), and MRI slice 5 of 9 (B) used to define the corresponding imaging landmark (yellow x). In the bottom row, the landmark positions are shown after registration overlaid on the MRI slice in transversal (C), sagittal (D) and coronal plane (E). Registration error for this landmark was 5 mm. (For interpretation of the references to color in this figure legend, the reader is referred to the web version of this article.)

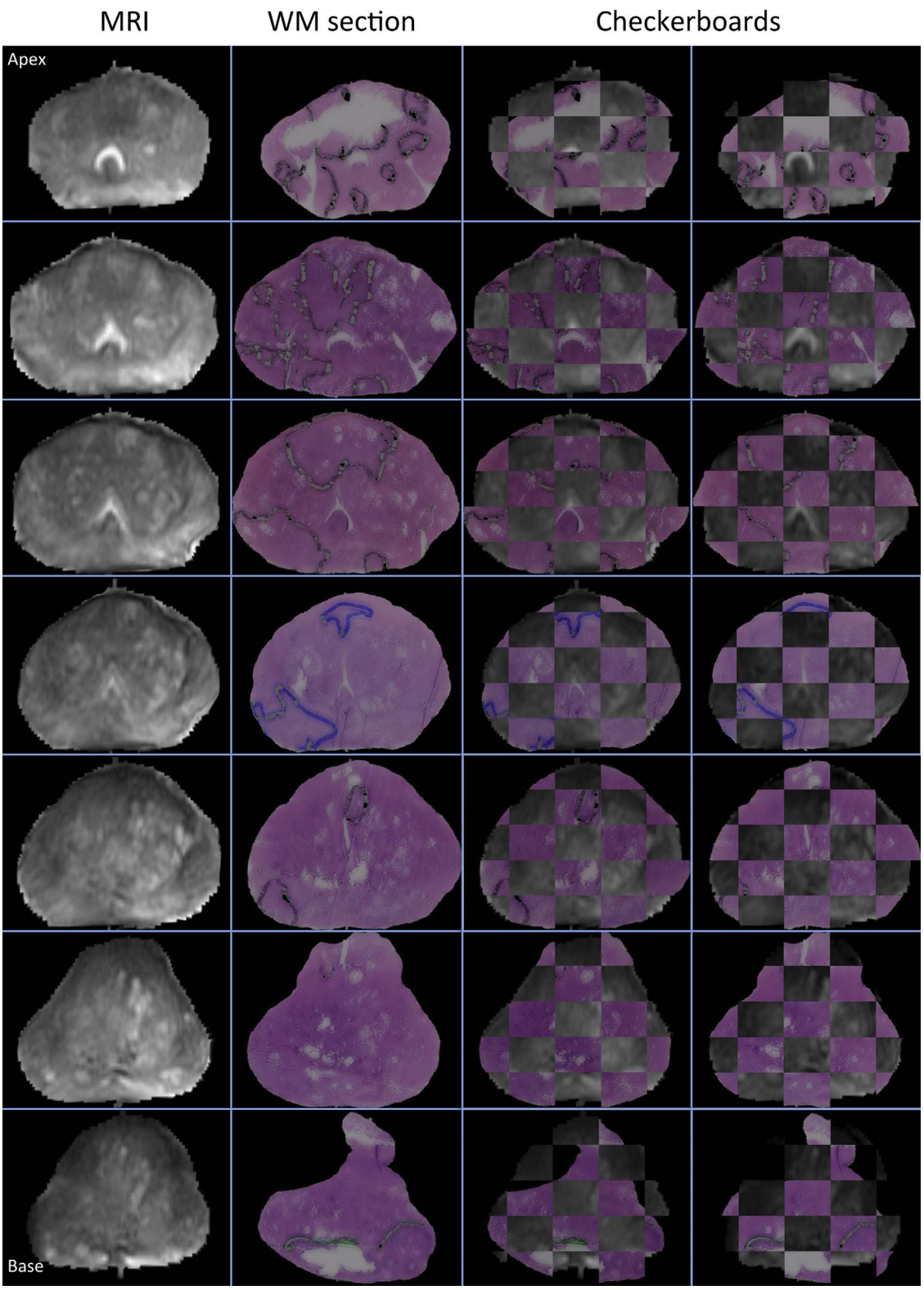

Fig. 4. Slicewise comparison of registered MRI (first column), and the corresponding WM sections (second column) for patient no. 8. First row show the slices closer to the apex, and last row closer to the base. Registration accuracy assessment using checkerboard images are shown in 3rd and 4th columns.

overlaps (DCs) for the whole prostate, somewhat lower for the remaining gland, and decent results for the peripheral zone. The peripheral zone is usually thinner than the spherical-shaped remaining gland, except in the apex. However, the apex was not normally captured by the transversal WM sections applied in our study, and therefore not included in the analysis. This can partly explain the inferior results for the peripheral zone, compared to the remaining gland. Several methods requiring more manual input and restricting validity to 2D have shown high accuracy, e.g. Kalavagunta et al. (2015) reported a registration accuracy of 1.5 mm using manually defined masks during the registration. Mazaheri et al. (2010) reported results in terms of 2D Dice Coefficients, and obtained DC = 0.91 for the whole prostate,

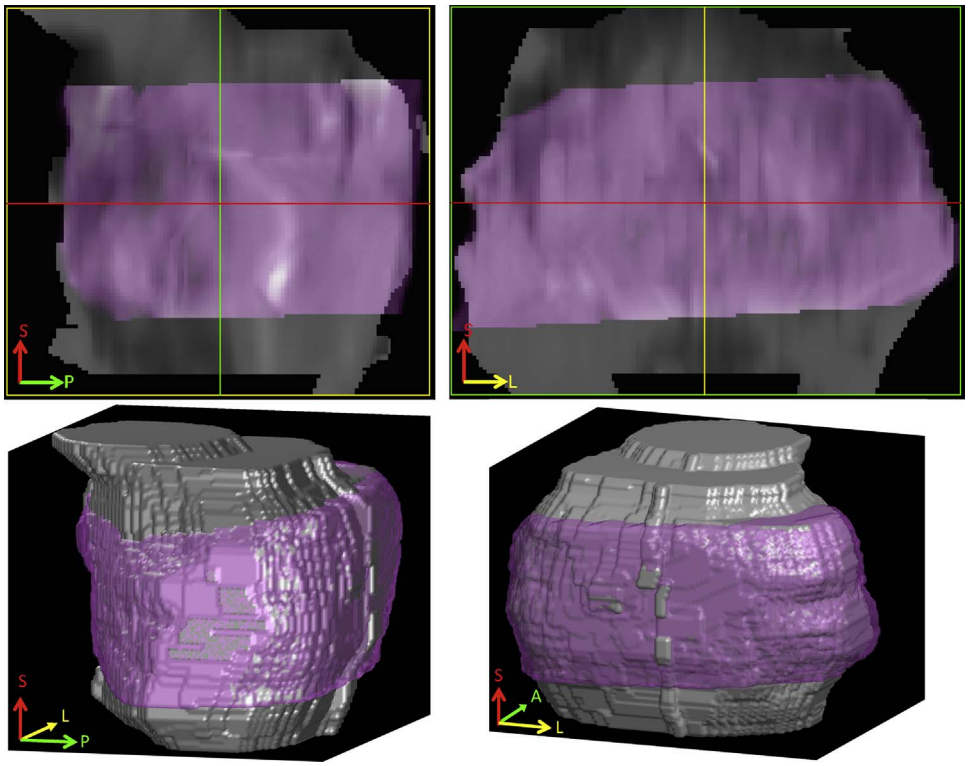

Fig. 5. Illustrations of the volume overlap and resulting slice angulations for patient no. 8. Sagittal view (left column) and coronal view (right column). The part of the prostate covered by the WM sections are shown in purple and the MRI is shown in grey. (For interpretation of the references to color in this figure legend, the reader is referred to the web version of this article.)

DC = 0.76 for the PZ and DC = 0.85 for the transition zone (TZ). Among 3D methods, Nir et al. (2014) reported an average DC of 0.87 for the whole prostate and landmark distances of about 3.8 mm, using *in vivo* MRI. Costa et al. (2017) obtained DCs of 0.85, 0.66 and 0.69 for the WG, PZ and TZ, respectively. With patient-specific 3D-printed molds the DCs increased to 0.94, 0.81 and 0.87, on average for two readers. Xiao et al. (2011) developed a method to automatically find the slice correspondences in MRI and WM sections, but their method did not involve possible differences in slice angle. Their quantitative results are not easily compared to ours, but they reported in most cases good slice correspondences when comparing the automated with a manual approach. Commandeur et al. (2015) reported a mean landmark distance of 4.9 mm, which is comparable to our results, but their method was evaluated on a much smaller number of patients (n = 3), compared to ours (n = 12).

In our sample, damaged or ruptured WM sections might have caused difficulties for the registration method. Tumor delineations on the WM section glass coverslips using ink might also have caused problems. We think these effects may explain the relatively large landmark distance for patient 1 (11.6 mm on average). Inclusion of gross prostate specimen has been proposed to solve these challenges (Groenendaal et al., 2010), but were not available in this study. Furthermore, we observed prostate deformations from the endorectal coil in some of the patients. These deformations seem to affect mostly the peripheral zone, which is located closest to the rectum. Such deformations might have been difficult for our method to overcome, and likely resulted in lower volume overlaps for the peripheral zone. There might also be additional deformations which are not compensated for in our method. However, 3D deformable registration between MRI and sparse WM sections is challenging. Involving more manual input to the method could have improved the registration accuracy, however the aim of the study was to keep manual input and time to complete the registration to a minimum. Regarding the evaluation of the performance of the registration method, manual segmentation of prostate zones may be challenging both in histopathology and MRI, and the definition of the landmarks may be subject to inter-observer variability, and might have influenced the results.

The use of whole mounts as a prerequisite for our study may represent a potential limitation for institutions not performing whole mounts as a standard procedure for radical prostatectomy specimens. However, in Europe a majority of pathology laboratories use total embedding of the prostate as a standard procedure, and more than half of these always use whole mounts (Egevad et al., 2008). In Norway all institutions performing radical prostatectomies use whole mount sectioning of the prostate routinely.

The mutual information (MI) was applied as similarity metric in our intensity-based approach. It is regarded as a good metric for multimodal image registration, but may also encounter challenges in some situations (Pluim et al., 2003; Dong et al., 2015). One of the challenges with registration of T2W-MRI and WM sections of the prostate, is that the peripheral zone is normally brighter than the remaining gland in MRI, while they are in the same intensity range in the WM sections. Other similarity metrics have been described in previous studies (Chappelow et al., 2011; Nir et al., 2014), but it was not in the scope of this work to compare different similarity metrics.

To further improve our results we plan to extend our approach with patient-specific molds (Costa et al., 2017; Trivedi et al., 2012) combined with *ex vivo* MRI. To make the proposed approach fully automated, our method could be combined with a segmentation method for the prostate and the prostate zones. Finally, successful MRI/histopathology co-registration like this method will enable tissue characterization and computer aided detection of tumor lesions and tumor grading using machine learning technologies.

5. Conclusion

We have presented a new registration workflow for aligning MRI recordings from patients with prostate cancer and histopathology WM sections of the excised prostate. Our method incorporates *a priori* knowledge about the MRI acquisition and preparations of the WM sections while addressing common challenges like slice correspondence, sparse data and differences in slice and imaging angle. Our method was found to be accurate and fast, and represents a new contribution to the important field of registration of mpMRI and

histopathology WM sections, with a wide range of clinical and research applications.

Conflict of interest

The authors declare no conflict of interest.

Acknowledgment

This work was supported by Helse Vest RHF, Norway (grant number 911862 to A. Losnegård.). The funder had no role in study design, data collection and interpretation, or the decision to submit the work for publication.

References

Avants, B.B., Tustison, N.J., Song, G., Cook, P.A., Klein, A., Gee, J.C., 2011. A reproducible evaluation of ants similarity metric performance in brain image registration. NeuroImage 54, 2033–2044. http://dx.doi.org/10.1016/j.neuroimage.2010.09.025.

Barentsz, J.O., Richenberg, J., Clements, R., Choyke, P., Verma, S., Villeirs, G., et al., 2012. ESUR prostate MR guidelines 2012. Eur. Radiol. 22 (4), 746–757.

Borren, A., Groenendaal, G., Moman, M.R., Boeken Kruger, A.E., van Diest, P.J., van Vulpen, M., et al., 2014. Accurate prostate tumour detection with multiparametric magnetic resonance imaging: dependence on histological properties. Acta Oncol. 53 (1), 88–95. http://dx.doi.org/10.3109/0284186X.2013.837581.

Chappelow, J., Bloch, B.N., Rofsky, N., Genega, E., Lenkinski, R., DeWolf, W., et al., 2011. Elastic registration of multimodal prostate MRI and histology via multiattribute combined mutual information. Med. Phys. 38 (4), 2005–2018.

Collignon, A., Maes, F., Delaere, D., D.V.P.S, Marchal, G., 1995. Automated multi-modality image registration based on information theory. In: Bizais, Y., Paola, C.B. (Eds.), Information Processing in Medical Imaging. Kluwer, Dordrecht, The Netherlands, pp. 263–274.

Commandeur, F., Acosta, O., Simon, A., Mathieu, R., Fautrel, A., Gnep, K., et al., 2015. Prostate whole-mount histology reconstruction and registration to MRI for correlating in-vivo observations with biological findings. Proc. 37th Annual Int. Conf. of the IEEE Engineering in Medicine and Biology Society (EMBC) 2399–2402. http://dx.doi.org/10.1109/EMBC.2015.7318877.

Costa, D.N., Chatzinoff, Y., Passoni, N.M., Kapur, P., Roehrborn, C.G., Xi, Y., et al., 2017. Improved magnetic resonance imaging-pathology correlation with imaging-derived, 3d-printed, patient-specific whole-mount molds of the prostate. Investig. Radiol. http://dx.doi.org/10.1097/RLI.0000000000000372.

Dice, L.R., 1945. Measures of the amount of ecologic association between species. Ecology 26 (3), 297–302.

Dong, C., Chen, Y.W., Seki, T., Inoguchi, R., Lin, C.L., Han, X.H., 2015. Non-rigid image registration with anatomical structure constraint for assessing locoregional therapy of hepatocellular carcinoma. Comput. Med. Imaging Graph 45, 75–83. http://dx.doi.org/10.1016/j.compmedimag.2015.08.003.

Egevad, L., Algaba, F., Berney, D.M., Boccon-Gibod, L., Griffiths, D.F., Lopez-Beltran, A., et al., 2008. Handling and reporting of radical prostatectomy specimens in Europe: a web-based survey by the European network of uropathology (enup). Histopathology 53, 333–339. http://dx.doi.org/10.1111/j. 1365-2559.2008.03102.x.

Gibson, E., Crukley, C., Gaed, M., Gomez, J.A., Moussa, M., Chin, J.L., et al., 2012. Registration of prostate histology images to ex vivo MR images via strand-shaped fiducials. J. Magn. Reson. Imaging 36 (6), 1402–1412. http://dx.doi.org/10.1002/jmri.23767.

Ginsburg, S.B., Viswanath, S.E., Bloch, B.N., Rofsky, N.M., Genega, E.M., Lenkinski, R.E., et al., 2015. Novel PCA-VIP scheme for ranking MRI protocols and identifying computer-extracted MRI measurements associated with central gland and peripheral zone prostate tumors. J. Magn. Reson. Imaging 41 (5), 1383–1393. http://dx.doi.org/10.1002/jmri.24676.

Groenendaal, G., Moman, M.R., Korporaal, J.G., van Diest, P.J., van Vulpen, M., Philippens, M.E.P., et al., 2010. Validation of functional imaging with pathology for tumor delineation in the prostate. Radiother. Oncol. 94 (2), 145–150. http://dx.doi.org/10.1016/j.radonc.2009.12.034.

Kalavagunta, C., Zhou, X., Schmechel, S.C., Metzger, G.J., 2015. Registration of in vivo prostate MRI and pseudo-whole mount histology using local affine transformations guided by internal structures (LATIS). J. Magn. Reson. Imaging 41 (4), 1104–1114. http://dx.doi.org/10.1002/jmri.24629.

Kimm, S.Y., Tarin, T.V., Lee, J.H., Hu, B., Jensen, K., Nishimura, D., et al., 2012. Methods for registration of magnetic resonance images of ex vivo prostate specimens with histology. J. Magn. Reson. Imaging 36 (1), 206–212. http://dx.doi.org/10.1002/jmri.23614.

Kitajima, K., Kaji, Y., Fukabori, Y., Yoshida, K.i., Suganuma, N., Sugimura, K., 2010. Prostate cancer detection with 3 T MRI: comparison of diffusion-weighted imaging and dynamic contrast-enhanced MRI in combination with T2-weighted imaging. J. Magn. Reson. Imaging 31 (3), 625–631. http://dx.doi.org/10.1002/jmri.22075.

Le Nobin, J., Orczyk, C., Deng, F.M., Melamed, J., Rusinek, H., Taneja, S.S., et al., 2014. Prostate tumour volumes: evaluation of the agreement between magnetic resonance imaging and histology using novel co-registration software. BJU Int. 114 (6b), E105–E112. http://dx.doi.org/10.1111/bju.12750.

Litjens, G.J.S., Elliott, R., Shih, N.N., Feldman, M.D., Kobus, T., Hulsbergen-van de Kaa, C., et al., 2015. Computer-extracted features can distinguish noncancerous confounding disease from prostatic adenocarcinoma at multiparametric MR imaging. Radiology 142856. http://dx.doi.org/10.1148/radiol.2015142856.

Mazaheri, Y., Bokacheva, L., Kroon, D.J., Akin, O., Hricak, H., Chamudot, D., et al., 2010. Semi-automatic deformable registration of prostate MR images to pathological slices. J. Magn. Reson. Imaging 32 (5), 1149–1157. http://dx.doi.org/10.1002/jmri.22347.

Nir, G., Sahebjavaher, R.S., Kozlowski, P., Chang, S.D., Jones, E.C., Goldenberg, S.L., et al., 2014. Registration of whole-mount histology and volumetric imaging of the prostate using particle filtering. IEEE Trans. Med. Imaging 33 (8), 1601–1613. http://dx.doi.org/10.1109/TMI.2014.2319231.

Orczyk, C., Rusinek, H., Rosenkrantz, A.B., Mikheev, A., Deng, F.M., Melamed, J., et al., 2013. Preliminary experience with a novel method of three-dimensional co-registration of prostate cancer digital histology and in vivo multiparametric MRI. Clin. Radiol. 68 (12), e652–e658. http://dx.doi.org/10.1016/j.crad.2013.07.010.

Park, H., Piert, M.R., Khan, A., Shah, R., Hussain, H., Siddiqui, J., et al., 2008. Registration methodology for histological sections and in vivo imaging of human prostate. Acad. Radiol. 15 (8), 1027–1039. http://dx.doi.org/10.1016/j.acra.2008.01.022.

Pluim, J.P.W., Maintz, J.B.A., Viergever, M.A., 2003. Mutual-information-based registration of medical images: a survey. IEEE Trans. Med. Imaging 22 (8), 986–1004. http://dx.doi.org/10.1109/TMI.2003.815867.

Reisæter, L.A., Fütterer, J.J., Halvorsen, O.J., Nygård, Y., Biermann, M., Andersen, E., et al., 2015. 1.5-T multiparametric MRI using PI-RADS: a region by region analysis to localize the index-tumor of prostate cancer in patients undergoing prostatectomy. Acta Radiol. 56 (4), 500–511. http://dx.doi.org/10.1177/0284185114531754.

Rosenkrantz, A.B., Verma, S., Choyke, P., Eberhardt, S.C., Eggener, S.E., Gaitonde, K., et al., 2016. Prostate magnetic resonance imaging and magnetic resonance imaging targeted biopsy in patients with a prior negative biopsy: a consensus statement by AUA and SAR. J. Urol. 196, 1613–1618. http://dx.doi.org/10.1016/j.juro.2016.06.079.

Rusu, M., Golden, T., Wang, H., Gow, A., Madabhushi, A., 2015. Framework for 3D histologic reconstruction and fusion with in vivo MRI: preliminary results of characterizing pulmonary inflammation in a mouse model. Med. Phys. 42 (8), 4822–4832. http://dx.doi.org/10.1118/1.4923161.

Singanamalli, A., Rusu, M., Sparks, R.E., Shih, N.N.C., Ziober, A., Wang, L.P., et al., 2015. Identifying in vivo DCE MRI markers associated with microvessel architecture and gleason grades of prostate cancer. J. Magn. Reson. Imaging. http://dx.doi.org/10.1002/jmri.24975.

Starobinets, O., Guo, R., Simko, J.P., Kuchinsky, K., Kurhanewicz, J., Carroll, P.R., et al., 2014. Semiautomatic registration of digital histopathology images to in vivo MR images in molded and unmolded prostates. J. Magn. Reson. Imaging 39 (5), 1223–1229. http://dx.doi.org/10.1002/jmri.24287.

Steenbergen, P., Haustermans, K., Lerut, E., Oyen, R., De Wever, L., Van den Bergh, L., et al., 2015. Prostate tumor delineation using multiparametric magnetic resonance imaging: inter-observer variability and pathology validation. Radiother. Oncol. 115 (2), 186–190. http://dx.doi.org/10.1016/j.radonc.2015.04.012.

Stille, M., Smith, E.J., Crum, W.R., Modo, M., 2013. 3D reconstruction of 2D fluorescence histology images and registration with in vivo MR images: application in a rodent stroke model. J. Neurosci. Methods 219 (1), 27–40. http://dx.doi.org/10.1016/j.jneumeth.2013.06.003.

Tiwari, P., Kurhanewicz, J., Madabhushi, A., 2013. Multi-kernel graph embedding for detection, gleason grading of prostate cancer via MRI/MRS. Med. Image Anal. 17 (2), 219–235. http://dx.doi.org/10.1016/j.media.2012.10.004.

Trivedi, H., Turkbey, B., Rastinehad, A.R., Benjamin, C.J., Bernardo, M., Pohida, T., et al., 2012. Use of patient-specific MRI-based prostate mold for validation of multiparametric MRI in localization of prostate cancer. Urology 79, 233–239. http://dx.doi.org/10.1016/j.urology.2011.10.002.

Turkbey, B., Albert, P.S., Kurdziel, K., Choyke, P.L., 2009. Imaging localized prostate cancer: current approaches and new developments. Am. J. Roentgenol. 192 (6), 1471–1480. http://dx.doi.org/10.2214/AJR.09.2527.

Viola, P., Wells III, W.M., 1995. Alignment by maximization of mutual information. In: Shafer, G.E.S., Blake, A., Sugihara, K. (Eds.), Int. Conf. Comput. Vis. Los Alamitos, CA, USA. pp. 16–23.

Vos, P.C., Barentsz, J.O., Karssemeijer, N., Huisman, H.J., 2012. Automatic computer-aided detection of prostate cancer based on multiparametric magnetic resonance image analysis. Phys. Med. Biol. 57 (6), 1527–1542. http://dx.doi.org/10.1088/0031-9155/57/6/1527.

Ward, A.D., Crukley, C., McKenzie, C.A., Montreuil, J., Gibson, E., Romagnoli, C., et al., 2012. Prostate: registration of digital histopathologic images to in vivo MR images acquired by using endorectal receive coil. Radiology 263 (3), 856–864. http://dx.doi.org/10.1148/radiol.12102294.

Xiao, G., Bloch, B.N., Chappelow, J., Genega, E.M., Rofsky, N.M., Lenkinski, R.E., et al., 2011. Determining histology-MRI slice correspondences for defining MRI-based disease signatures of prostate cancer. Comput. Med. Imaging Graph 35 (7–8), 568–578. http://dx.doi.org/10.1016/j.compmedimag.2010.12.003.

Yushkevich, P.A., Piven, J., Hazlett, H.C., Smith, R.G., Ho, S., Gee, J.C., et al., 2006. User-guided 3d active contour segmentation of anatomical structures: significantly improved efficiency and reliability. NeuroImage 31, 1116–1128. http://dx.doi.org/10.1016/j.neuroimage.2006.01.015.

Zhan, Y., Ou, Y., Feldman, M., Tomaszeweski, J., Davatzikos, C., Shen, D., 2007. Registering histologic and MR images of prostate for image-based cancer detection. Acad. Radiol. 14 (11), 1367–1381. http://dx.doi.org/10.1016/j.acra.2007.07.018.